Dalton Transactions

The Binuclear Copper State of Peptidylglycine Monooxygenase Visualized through a Selenium-Substituted Peptidyl-Homocysteine Complex

Journal:	*Dalton Transactions*
Manuscript ID	DT-ART-01-2025-000082.R1
Article Type:	Paper
Date Submitted by the Author:	02-Feb-2025

Complete List of Authors:	Blackburn, Ninian; Oregon Health & Science University, Department of Chemical Physiology and Biochemistry Welch, Evan; Oregon Health & Science University, Department of Chemical Physiology and Biochemistry Rush, Katherine ; Oregon Health & Science University, Department of Chemical Physiology and Biochemistry; Auburn University, Department of Chemistry and Biochemistry Eastman, Karsten ; The University of Utah Department of Chemistry, Department of Chemistry Bandarian, Vahe; The University of Utah Department of Chemistry, Department of Chemistry

The Binuclear Copper State of Peptidylglycine Monooxygenase Visualized through a Selenium-Substituted Peptidyl-Homocysteine Complex

Evan F. Welch§, Katherine W. Rush§†, Karsten A. S. Eastman‡, Vahe Bandarian‡ and Ninian J. Blackburn§*

§Department of Chemical Physiology and Biochemistry, Oregon Health and Sciences University, Portland, OR 97239 USA

† Department of Chemistry and Biochemistry, Auburn University, Auburn, AL 36849 USA

‡Department of Chemistry, University of Utah, Salt Lake City, UT 84112, USA

* To whom correspondence should be sent

Submitted to Chemical Science

Supplementary Information available: Four figures and two tables containing details of LCMS analysis of the selenopeptide, additional EXAFS data, PHM activity, selenomethionine-containing peptide reactivity, quantitative EPR analysis and EPR simulation parameters. See DOI:

Abstract. Bioactive peptides generally require post-translational processing to convert them to their fully active forms. Peptidylglycine monooxygenase (PHM) is a copper-dependent enzyme that catalyzes C-alpha hydroxylation of a glycine-extended pro-peptide, a critical post-translational step in peptide amidation. A canonical mechanism based on experimental and theoretical considerations proposes that molecular oxygen reacts at the mononuclear CuM-center to form a reactive Cu(II)-superoxo intermediate capable of H-atom abstraction from the peptidyl substrate, followed by long range ET from the CuH center positioned 11 Å away across a solvent-filled cleft. However, recent data has challenged this mechanism, suggesting instead that an “open-to-closed” conformational transition brings the copper centers closer to facilitate reaction at a binuclear copper site. Here we present direct observations of an enzyme-bound binuclear copper species, which was enabled by the use of an Ala-Ala-Phe-homoselenocysteine (hSeCys) species. EXAFS, UV/vis, and EPR studies are used to show that this reagent reacts with the oxidized enzyme to form a novel mixed valence entity which is subtly different from that observed previously for the S-peptidyl complex (J. Am. Chem. Soc. (2024)146, 5074-5080). In the ascorbate-reduced Cu(I) state of PHM, EXAFS measurements at both the Se and Cu absorption edges provide a unique signature of a bridging mode of binding, with Se-Cu site occupancy (1.8) measured from the Se-EXAFS simulating to twice that of the Cu-Se site occupancy (0.85) measured at the Cu edge. The ability of the hSeCys entity to induce a binuclear state is further emphasized by the XAS of the selenomethionyl peptide complex, where no such bridging chemistry is observed. The properties of the binuclear PHM derivative are of interest due to their unique chemical signatures, as well as providing the basis for a completely new mechanistic paradigm for PHM and its monooxygenase congeners.

Introduction.

The mechanism of action of copper monooxygenases has attracted attention due to the role of these enzymes in important biological processes such as hormone biosynthesis, climate mitigation and peptide processing. Peptidylglycine monooxygenase (PHM) [1, 2] and its sister enzymes dopamine β monooxygenase (DBM) and tyramine β monooxygenase (TBM) [3, 4] catalyze the biosynthesis of neuropeptide hormones and catecholamine neurotransmitters respectively and thus play central roles in the regulation of bodily functions including the endocrine and sympathetic nervous systems. X-ray crystal structures reveal that the enzymes share a common active site composed of a pair of copper atoms termed CuH and CuM which in the resting oxidized enzymes are separated by ~11-14 Å across a solvent-filled cleft (Scheme 1(a)) [5, 6]. CuH is coordinated by three His residues (H107, H108, H172 PHM numbering) while CuM is coordinated by two histidines and a methionine residue (H242, H244, M314 PHM numbering), Scheme 1(b). Very recently a related enzyme class has been described named the BURP domain which catalyzes cyclization of ribosomally synthesized and posttranslationally modified peptides (RiPPs) using a pair of mononuclear copper centers with coordination similar to the PHM M-center. [7] Understanding the detailed mechanism of these enzymes thus continues to garner significant attention.

Extensive spectroscopic[8-12], kinetic[3, 13-17] and computational[18-22] studies on PHM have made it the system of choice for detailed mechanistic studies. Here, a C-terminal glycine-extended pro-peptide undergoes initial hydroxylation at the glycine α-C to form an α-hydroxyglycine intermediate (Scheme 1(c)), which is further processed by a second enzymatic activity (peptidylglycine α-hydroxylating lyase, PAL) to generate the amidated peptide product. Substrate-bound structures visualize the peptidylglycine substrate bound to R240 and Y318 via its C-terminal carboxylate (Scheme 1(b)) which brings the α-C into the proximity of the CuM center. Using the slow substrate tyrosyl-D-threonine, Amzel and coworkers obtained a structure

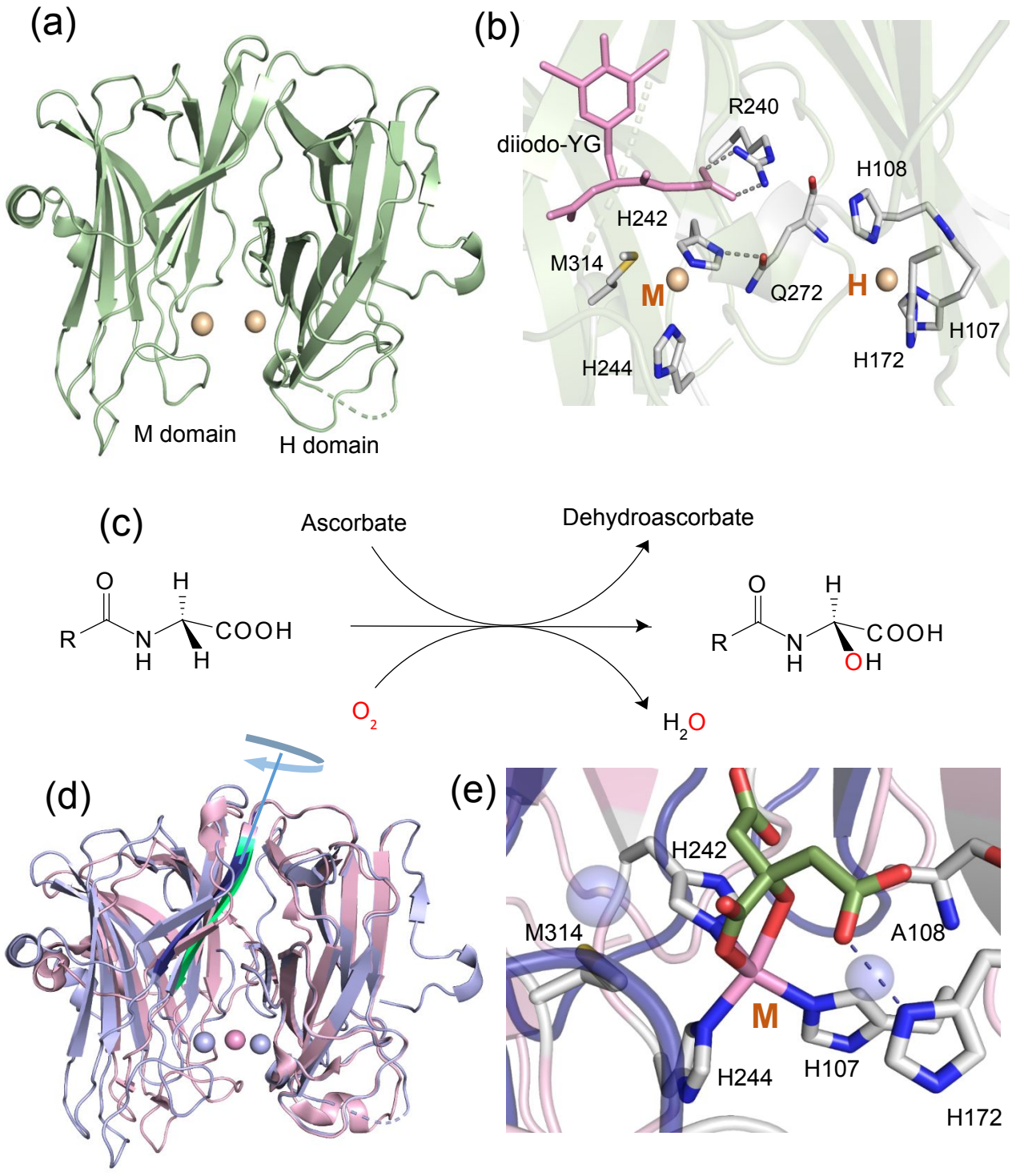

Scheme 1. Structure and reactivity of peptidylglycine monooxygenase (PHM). (a) 2-domain structure of showing the H- and M-domains each binding a Cu atom separated by ~11 Å (b) active site structure showing the coordination environment of the CuH and CuM and the position of the bound substrate di-iodo-tyrosylglycine (c) reaction catalyzed by PHM (d) sub-domain movement about I201generating open and closed states of PHM with either long (11-14 Å) or short (4-5 Å) Cu-Cu distances (e) closed conformer of PHM showing the singly bound CuM in pink coordinated by three M-site and 1 H-site ligands. The positions of the Cu centers in the open structure are shown as decolorized blue spheres. Reproduced using PDB files 3PHM ((a) and (b)), 3PHM, 6ALA, and 8DSJ (d) and 6ALA (e).

of an oxygen adduct bound to CuM but with the $^4O_2$ in an unproductive conformation pointing

away from the substrate C-alpha.[23] Based on these studies, a canonical "mononuclear" mechanism for substrate hydroxylation was proposed[18-20] in which the substrate-bound Cu(I) enzyme reacts with dioxygen at the CuM site to form a Cu(II)M-superoxo intermediate capable of extracting the pro-S H atom from the glycyl C-alpha methylene group to form a substrate radical. The catalytic cycle is completed by a long-range electron tunneling (ET) event from CuH or via formation of a Cu(II)M-oxyl intermediate.

The mononuclear or "canonical" mechanism is based on the assumption derived from early crystal structures that the two sub-domains that harbor the CuH and CuM centers are locked into a conformation that precludes any change in the 11 Å Cu-Cu distance. However, a number of structures challenging this premise have emerged recently both for PHM[24, 25] and DBM[6] in what have been termed fully open (Cu-Cu = 14 Å) and closed conformations (Cu-Cu = 4 – 5 Å). A closed conformation for the PHM variant H108A is shown in Scheme 1(d,e) where the M domain has rotated relative to the H domain about a hinge residue (I201) located on the interdomain loop which brings the copper centers closer together. This structure lacks the CuH metal ion and instead, the CuM is coordinated by two M-site histidines, one H-site histidine and a citrate molecule. The occurrence of both open and closed structures suggests flexible dynamics between the two copper-containing sub-domains which may allow the Cu-Cu distance to vary continuously,[25] raising the possibility that binuclear states of the enzyme might contribute to the reaction coordinate. This idea has been explored computationally for DBM [22] and found to be energetically plausible with two specific attributes, first that the energy of conversion from open to closed conformer is a mere 2 kcal mol^{-1}, and second that the reactive species is a hydroperoxo-bridged mixed valence dinuclear complex.

For these reasons we sought a method of probing the conformational landscape of PHM with the goal of isolating binuclear states that could be characterized spectroscopically. Recently we communicated an initial report of the chemistry and spectroscopy of complexes of

oxidized and reduced PHM with the peptidyl inhibitor Ala-Ala-Phe-homocysteine (AAF-hCys) [26]. This study was based on the concept that this bifunctional peptidyl substrate analogue could react at the carboxylate binding site in the vicinity of CuM but would also be capable of capturing the H-site Cu via coordination of its thiolate to both CuM and CuH forming a thiolate bridge that would induce the open to closed transition. This chemistry was indeed observed and validated by EXAFS spectroscopy. In addition, reaction of AAF-hCys with the fully oxidized enzyme generated an unusual mixed valence (MV) complex with an intervalence charge transfer band at 925 nm. The latter observation was significant given the evidence for the intermediacy of such a species from QM/MM [22].

In the present paper we explore the chemistry of formation of the binuclear state in detail using the Se analogue Ala-Ala-Phe-homoselenocysteine (AAF-hSeCys). Substitution with the heavier chalogenic congener has allowed the characterization of reduced forms using X-ray absorption (XAS) at both Cu and Se edges, where the requirement for structural mirroring in the X-ray absorption fine structure (EXAFS) data provides more accurate description of the complexes. Further, differences in redox potential between S and Se homocysteine analogues lead to perturbation of both the spectroscopy and stability of the MV species. The results expand and fully validate the chemistry and spectroscopy of the binuclear states of PHM presented in our earlier communication.

Results

We recently described the reaction of the AAF-hCys (S-thiol) peptide with oxidized PHM to generate a localized mixed valence species, and with reduced PHM to form the thiolate-bridged dinuclear complex characteristic of the closed conformer.[26] The S-containing peptide was synthesized as the reduced thiol with only small (<10 percent) contribution from the disulfide form and therefore underwent reactivity with both oxidized and reduced PHM without the need for further treatment. The monomeric form of the Se analogue (AAF-hSeCys) was synthesized by solid-phase peptide synthesis; however, during cleavage and deprotection, the highly reactive selenol rapidly oxidized, resulting in the diselenide as the primary species present after purification (Figure S1), which did not react with either redox state of the enzyme unless first reduced to the selenol form.

HPLC-HRMS Characterization of the AAF-hSeCys Diselenide Peptide. The diselenide $(AAF\text{-}hSeCys)_2$ eluted as a single peak from 7.75 to 7.95 minutes, as shown in the HPLC chromatogram trace (Figure S1(a)). Analysis of the high-resolution mass spectrometry (Figure S2(b) and S2(c)) data revealed two charge states present in the mass spectrum: a doubly charged species (z = 2) and a singly charged species (z = 1). The expected monoisotopic mass (m/z) for the z = 2 charge state is 472.1219, while the observed monoisotopic mass is 472.1207, resulting in a ppm error of -2.54. For the z = 1 charge state, the expected monoisotopic mass is 943.2366, with the observed monoisotopic mass being 943.2362, yielding a ppm error of -0.81.

Reduction of the AAF-hSeCys Diselenide to its Reactive Selenol Form. Reduction of the AAF-hSeCys diselenide proved to be challenging since the Se-Se bond is more stable than the homologous disulfide and requires stronger reductants. X-ray absorption spectroscopy at the Se edge provided a convenient method for studying the progress of reduction by various reagents. The Fourier transform (FT) of the starting diselenide-containing material showed a

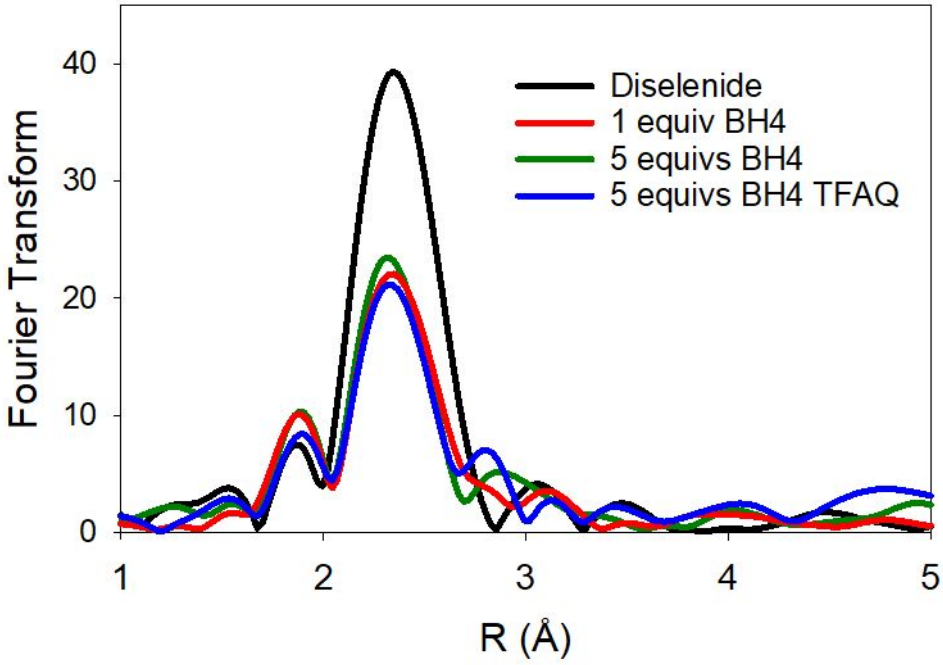

Figure 1. Se edge phase-corrected Fourier transforms of the AAF-hSeCys peptide treated with various reductants. 1 mM peptide in anhydrous with sodium borohydride in the same solvent. Black trace untreated diselenide; red trace + 1 molar equivalent $NaBH_4$; green trace + 5 molar equivalents $NaBH_4$; blue trace + 5 molar equivalents $NaBH_4$ after quenching with TFA

weak first shell peak due to the Se-C at ~1.95 Å, and an intense second shell feature at 2.31 Å due to the Se-Se interaction of the diselenide covalent bond (Figure 1 (black trace)) with intensity that is expected to decrease as the diselenide is reduced. In aqueous buffer, reduction by dithiothreitol (DTT) was about 30 percent effective in reducing the diselenide but TCEP and sodium borohydride were ineffective (Figure S2). The most effective reductant in aqueous medium was sodium dithionite which led to complete reduction at 50 mM but almost no reduction at concentrations (12.5 mM) suitable for enzyme studies (Figure S2). We also considered the effect of high concentrations of dithionite and borohydride on the activity of PHM, since small molecule reductants could not effectively be removed from the peptide reagent and must therefore be benign relative to the enzyme activity. Both were lethal to the enzyme (Figure S3), possibly via a mechanism that reduces the 5 critical disulfide linkages and denatures the protein.

Against this background, we explored alternative approaches. Borohydride is known to undergo degradation in aqueous media via protonation of the hydride ion, and generation of hydrogen gas, but an aprotic environment could lead to effective reduction. Reaction of one equivalent of $NaBH_4$ in anhydrous DMSO with the AAF-hSeCys in the same solvent led to ~ 30 percent reduction (Figure 1 red trace) to the selenol. 5-fold excess of $NaBH_4$ should in principle lead to full reduction but under the same experimental conditions did not appear to increase the percent of reduced selenol (Figure 1 green trace). Additionally, excess borohydride was undesirable due to its inhibitory effect on the enzyme. We tested whether it could be removed from the peptide by treatment with trifluoroacetic acid (TFA) in anhydrous DMSO. In a test reaction 50 mM AAF-hSeCys in anhydrous DMSO was reacted with a 5-fold excess of $NaBH_4$ and the reduction allowed to proceed for 30 minutes. The resulting reaction mixture was then titrated with small aliquots of TFA diluted in anhydrous DMSO. Addition of 1 equivalent of TFA led to vigorous evolution of gas (H_2 + B_2H_6) which was allowed to subside before further TFA addition. An additional 0.2 equivalents of TFA produced a solution that no longer effervesced on further TFA addition. The FT of this solution at the Se edge showed approximately 50 percent reduction (Figure 1 blue trace) similar to the result without TFA quench. Currently we do not have an explanation for why excess BH_4^- does not appear to increase the extent of reduction, but (*vide infra*) it is possible that the selenol is initially fully reduced by the excess borohydride, and that the observed residual diselenide results from reoxidation due to dilution into the measurement buffer (50 mM phosphate + 20% ethylene glycol). This TFA-quenched solution was used for further studies.

Reaction of the selenol form of AAF-hSeCys with fully reduced PHM. Ascorbate-reduced Cu(I)-containing PHM was reacted with borohydride-reduced TFA-quenched AAF-hSeCys and the identity of the product analyzed by XAS at both the Se and Cu edges. Data from two absorption edges have the advantage that metrical details (coordination numbers, distances and Debye Waller (DW) factors) due to Se-Cu interactions at the Se edge must exactly mirror those due to Cu-Se at the Cu edge. For a Se-bridged dicopper species, we expect each Se to

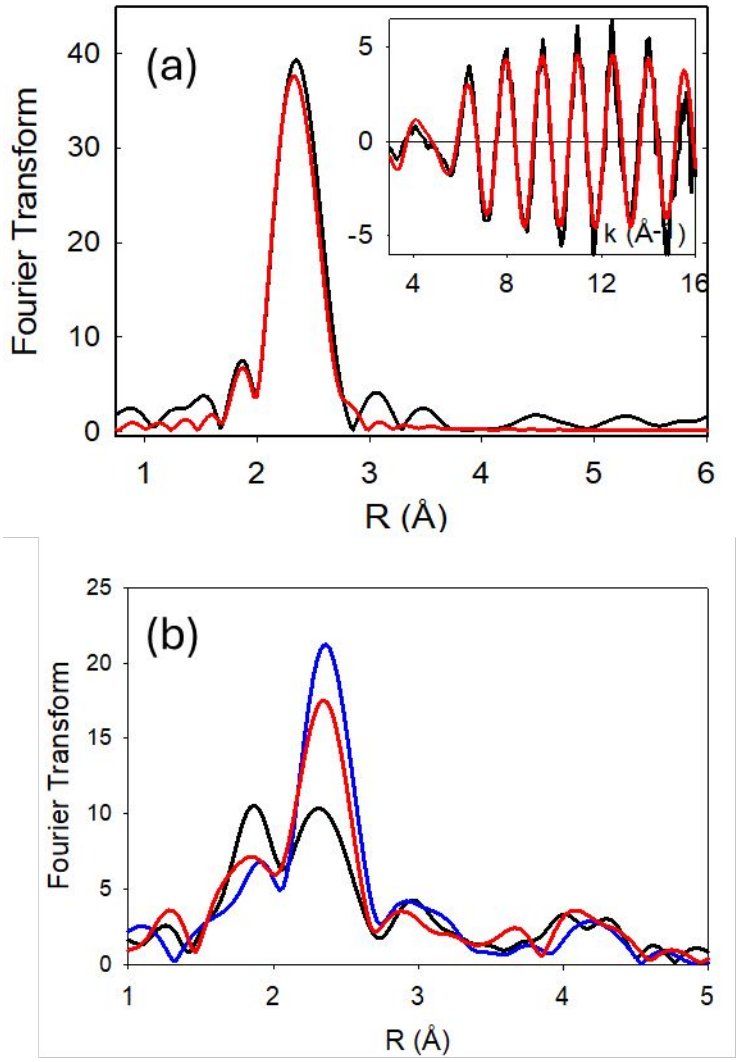

Figure 2. (a) Se edge Fourier transform and EXAFS (inset) for the diselenide form of the AAF-hSeCys peptide. The black trace represents experimental data, the red trace represents simulated data. Parameters used in the fit are listed in Table 1. (b) Cu edge Fourier transforms for reaction of ascorbate-reduced Cu(I) PHM with different preparations of AAF-hSeCys peptide reduced with varying stoichiometries of TFA-quenched $NaBH_4$: black trace 1 equivalent of peptide reduced with 1 equivalent $NaBH_4$; red trace 2 equivalents of peptide reduced with 1 equivalent $NaBH_4$; b trace 1 equivalent of peptide reduced with 5 equivalents $NaBH_4$.

Table 1. Parameters used in the fits to EXAFS data.

Selenium edge		**Se-C**				**Se-Se**				**Se-Cu**				
	F[1] (x10^{-3})	**No[2]**	**R (Å)[3]**	**DW (Å^2)[4]**		**No**	**R (Å)**	**DW (Å^2)**		**No**	**R (Å)**	**DW (Å^2)**		**ΔE_0**
AAF-hSeCys peptide diselenide	1.08	1	1.97	0.006		1.0	2.32	0.003		-	-	-		-4.03
AAF-hSeCys reduced borohydride quenched	4.1[5]	1	1.97	0.007		0.5	2.33	0.003						-3.0
redPHM + AAF-hSeCys	0.65	1	1.96	0.007		0.1	2.31	0.003		1.8	2.39	0.008		-3.2
redPHM + AAF-SeMet	2.8	2	1.96	0.007						1	2.41	0.012		-5.7
Copper edge		**Cu-N(His)[6]**				**Cu-S**				**Cu-Se**				
	F (x10^{-3})	**No**	**R (Å)**	**DW (Å^2)**		**No**	**R (Å)**	**DW (Å^2)**		**No**	**R (Å)**	**DW (Å^2)**		**ΔE_0**
redPHM + AAF-hSeCys	0.46	2	1.93	0.020		0.5	2.21	0.011		0.85	2.38	0.008		-3.0
redPHM + AAF-SeMet	0.54	2	1.91	0.011		0.5	2.25	0.013		0.5	2.41	0.010		-0.32
oxPHM + AAF-hSeCys	0.50	2.5	1.95	0.011		0.5	2.20	0.013		0.7 0.3	2.41 2.84	0.012 0.016		-1.13

[1] F is a least-squares fitting parameter defined as $F^2 = \frac{1}{N}\sum_{i=1}^{N} k^6(Data - Model)^2$. The larger value of F for Se arises from data [6]

[2] Coordination numbers are generally considered as accurate +/- 25% unless indicated as low confidence.

[3] In any one fit, the statistical error in bond-lengths is ±0.005 Å. However, when errors due to imperfect background subtraction, phase-shift calculations, and noise in the data are compounded, the actual error is probably closer to ±0.02 Å.

[4] Debye-Waller (DW) factors are reported as $2\sigma^2$ and are defined as twice the mean square deviation of the experimental bond distance as compared to the simulated value.

[5] Noisy data

[6] Imidazole rings were simulated using full multiple scattering from C2/C5 at 127^0 and C3/N4 at 163^0 from the Cu-N axis. Cu-C2/C5 = 2.78, 3.01 Å; Cu-N4/C5 = 4.03, 4.21 Å. The split shells approximate the average distortion of the imidazole plane from the Cu-N axis.

"see" two Cu scatterers at the Se edge, while each Cu should "see" one Se scatterer at the Cu edge. Analysis of the Se edge data is complicated by the potential presence of residual diselenide in the sample: Se-Se interactions typically have Se-Se bond lengths of 2.31 Å while Se-Cu bond lengths are typically around 2.40 Å [27, 28] which can introduce ambiguity in the accurate determination of Se-Cu occupation numbers unless the relative contributions of both species are known. To address this problem, we analyzed the Se EXAFS data in terms of a chemical model that assumes that only two distinguishable Se species are present – the Se bridged dicopper PHM complex with EXAFS contributions from 2 Se-Cu interactions and the diselenide form of the peptide with EXAFS contributions from 1 Se-Se interactions. Since the EXAFS amplitudes are normalized to the total Se in the sample, the Se-Cu shell-occupancy N_{Cu} is related to the Se-Se shell occupancy by the following equation

$$N_{Cu} = 2(1 - N_{Se}) \quad \ldots (1)$$

Since the Se-Se distance and Debye-Waller (DW) factor for the Se-Se shell are known from simulation of the free diselenide (Figure 2 (a) and Table 1), this simple relationship allows the best estimate for the ratio of Se-Se and Se-Cu species to be determined. To test the approach, we first measured data from samples where the anticipated Se-bridged complex was not fully formed. As mentioned above, reaction of 1 equivalent of $NaBH_4$ with AAF-hSeCys followed by a TFA quench produced a mixture where the peptide was 30 percent reduced. Therefore, reacting this reagent 1:1 or 2:1 with enzyme was expected to produce N_{Cu} values of 0.6, and 1.2 respectively. (Note that the 2:1 sample was passed through two spin columns to remove excess peptide). Figure 2(b) shows FT data at the Cu edge for each of these samples where the Cu-Se shell intensity is seen to increase from ~30 percent to ~60%. These values were confirmed by simulation at both edges (Table S1). Refinement of the 2:1 sample gave a best fit 1.2 Cu per Se with R_{Se-Cu} = 2.39 Å and DW factors $2\sigma^2$= 0.007 A^{-1} mirrored at the Cu edge but

with shell occupancies that differed by half, providing validation of both the fitting approach and the chemical model.

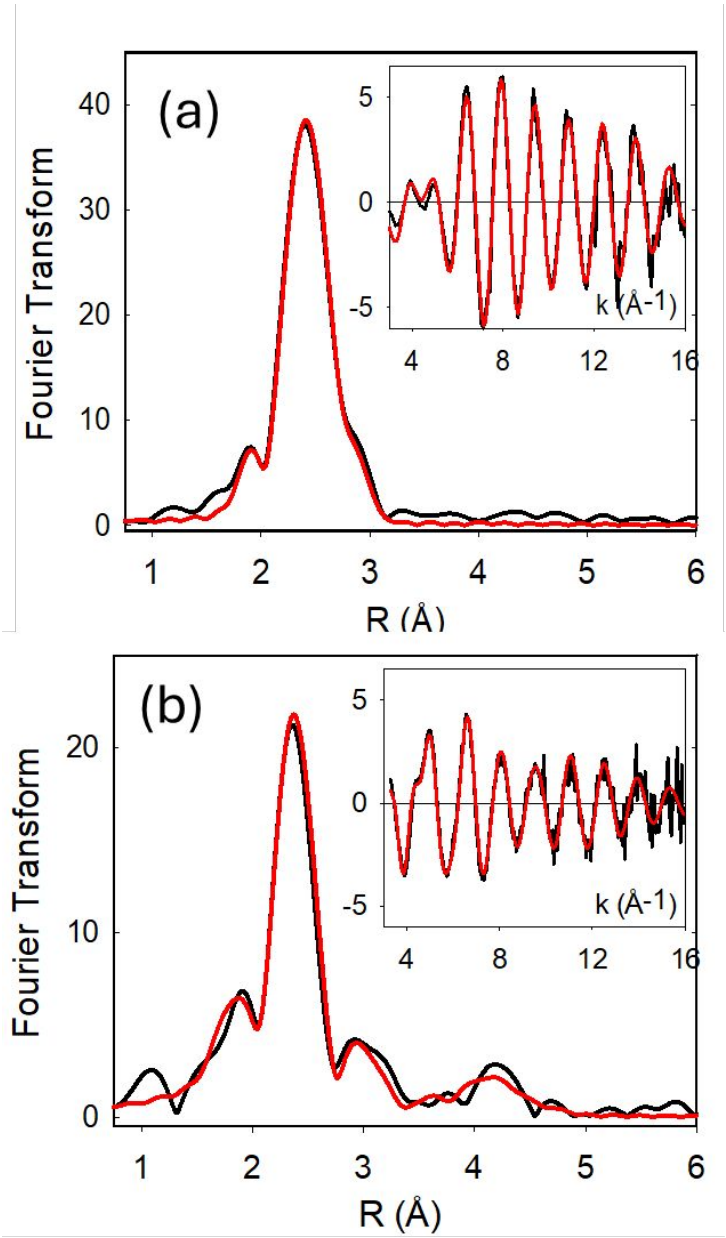

Figure 3. Fourier transforms and EXAFS (insets) for (a) the Se and (b) the Cu K EXAFS of ascorbate-reduced Cu(I) PHM reacted with 1 equivalent of AAF-hSeCys. The peptide was reduced with 5 equivalents of $NaBH_4$ which was subsequently quenched with TFA as described in the text. Black traces are experimental data, red traces are simulated data. Parameters used in the fits are listed in Table 1.

Our final experiments with the ascorbate-reduced PHM utilized the selenol reduced with 5-fold excess of $NaBH_4$ followed by TFA quenching. We reacted the selenol with reduced PHM at either 1:1 or 2:1 ratio followed by purification with two sequential spin desalting columns

(7kDa MWCO) to remove excess unbound peptide. Analysis by ICP-OES gave a Cu:Se ratio of 2:1 showing binding of one peptide to the protein. Both procedures generated identical EXAFS spectra. The data and their simulations for the 1:1 addition are shown in Figure 3(a) at the Se edge and Figure 3(b) at the Cu edge. Simulations (Table 1) showed that the Se-bridged species was formed to ~85 percent in each case with Se-Cu and Cu-Se distances and DW factors again mirrored at each edge ($R_{Cu\text{-}Se}$= 2.39 Å, $DW_{Cu\text{-}Se}$= 0.008 $Å^{-1}$). The N_{Cu} value of 1.8 mirrored by half this value at the Cu edge provides unambiguous evidence for the formation of the selenolate bridge, and hence the formation of the dinuclear Cu(I) species of the closed conformer.

Control Reaction with AAF-SeMet. As a further test of the formation of the Se-bridged dinuclear state by the AAF-hSeCys peptide we studied the reaction with the homologous peptide containing a C-terminal selenomethionine residue (AAF-SeMet). The substitution of the strongly coordinating negatively charged selenolate donor group with the weaker neutral selenoether was expected to perturb or eliminate the open to closed transition, since the coordinating power of the SeMet ligand would be fully satisfied by binding at the CuM site. Figures 4 (a) and (b) show the EXAFS at the Se and Cu edges for a sample of ascorbate-reduced PHM reacted with 3 equivalents of AAF-SeMet followed by 2 spin columns to remove excess peptide. Analysis by ICP-OES gives a Cu:Se ratio of 2:1, similar to that obtained for the AAF-hSeCys showing binding of one peptide to the protein. However, the Se-Cu and Cu-Se occupation numbers at the Se and Cu edges respectively are now different, with Se “seeing” 1 Cu and Cu “seeing” 0.5 Se. Metrical details for these simulations are given in Table 1. This result is consistent with the AAF-SeMet peptide binding via its carboxy terminus to the R240/Y318 substrate-binding diad but forming only 1 additional linkage to a Cu atom, which we speculate is the CuM center. Thus, when the coordinating power of the peptidyl lure is decreased it can no longer capture the H-domain and induce domain closure.

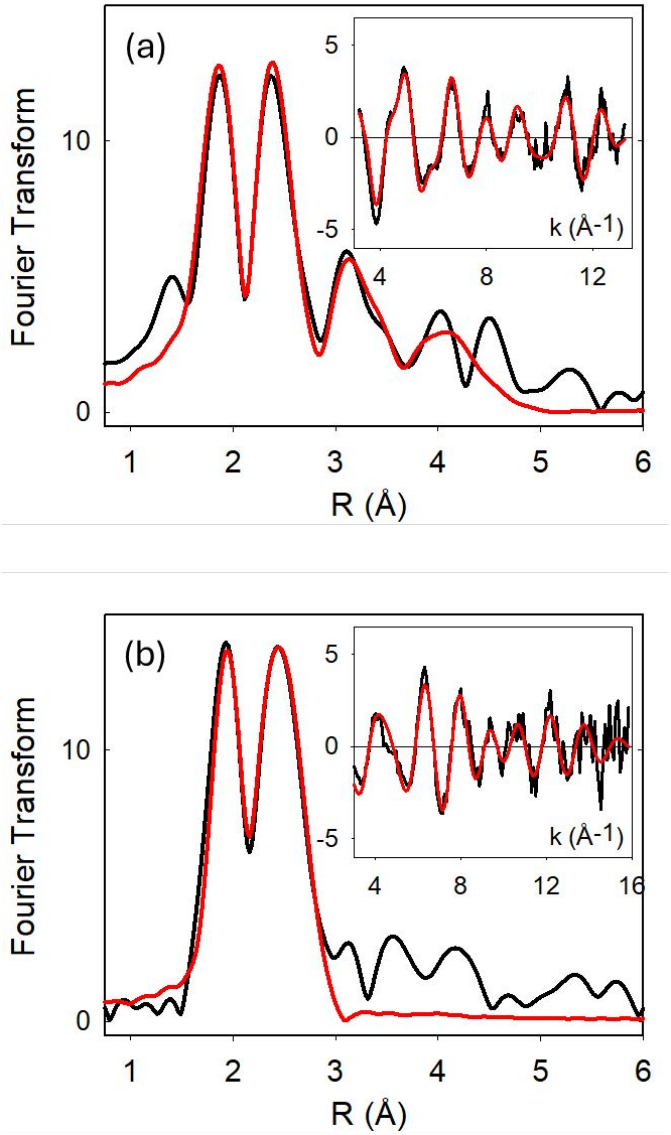

Figure 4. Fourier transforms and EXAFS (insets) for reaction of AAF-SeMet with ascorbate-reduced Cu(I) PHM. (a) Cu edge data (b) Se edge data. Black traces are experimental data, red traces are simulated data. Parameters used in the fits are listed in Table 1.

Reaction of the selenol peptide with oxidized PHM. In a previous communication we reported the reaction of the AAF-hCys S-containing peptide with oxidized PHM.[26] The broad NIR peak at ~925 was provisionally assigned as an intervalence charge transfer band (IVCT) by comparison with other mixed valence systems, [29-37] and from EPR analysis which showed equal concentrations of Cu(II) and Cu(I) in the purple species. It was argued that this must imply an interaction between a Cu(I) and a Cu(II) center leading to electron exchange in the excited state. Studies of the EPR characteristics of this species indicated that it was a class II IVCT

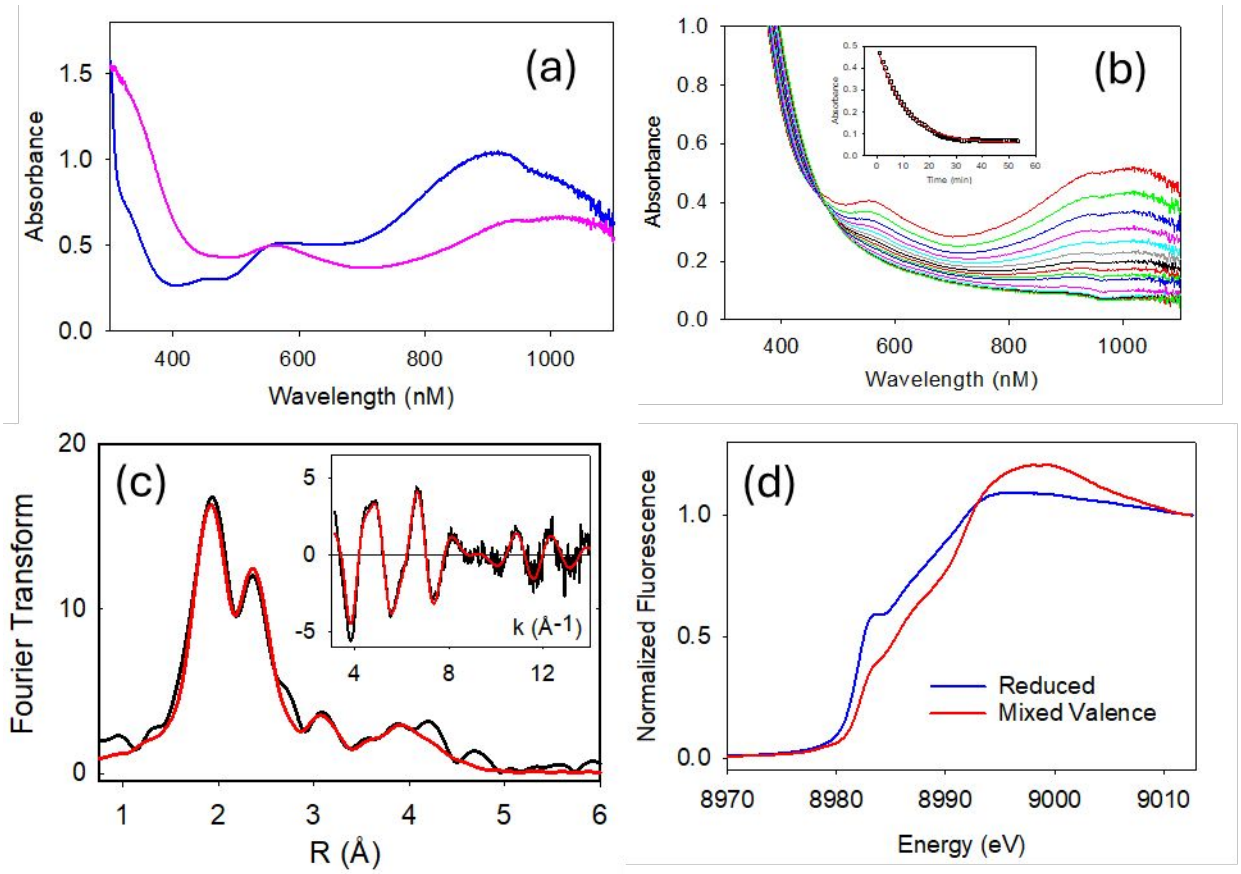

Figure 5. Reaction of the AAF-hSeCys peptide with oxidized Cu(II) PHM to form the mixed valence complex. (a) Comparison of UV/vis spectra of the mixed valence complexes of PHM with AAF-hCys (pink) and AAF-hSeCys (blue) showing the intervalence charge transfer band of the selenohomocysteine MV complex red-shifted from 925 nm to 1000 nm. Extinction coefficients are calculated as described in the text and listed in Table S2 (b) reduction of the MV complex formed with AAF-hSeCys with 5 mM ascorbate in a pseudo first order decay with k_{obs}=0.1 s^{-1} (c) Fourier transform and EXAFS (inset) for the Cu edge of the seleno MV complex (parameters in Table 1) (d) comparison of the Cu K absorption edges of the MV (red) and reduced (blue) complexes of PHM-AAF-hSeCys complexes.

system where the electron exchange was sufficiently slow that the two sites were valence localized on the time scale of the EPR absorption. This contrasted with other well-known IVCT systems such the CuA sites of cytochrome oxidase, purple Cu azurin, and N_2O reductase (λ_{max} = 460, 530, 795 nm)[31-38] where the electron exchange is rapid, and leads to full delocalization over both Cu nuclei. In CuA, the double cysteine bridge forms the $[(Cu)_2S_2]^{3+}$ diamond core with a short (2.4 Å) Cu-Cu distance, and a significant proportion of direct Cu-Cu bonding[35, 39] which is believed to be the conduit for the electron delocalization. In the PHM case, this mode of bridging is clearly absent, yet the presence of a IVCT band would still require formation of a

ligand bridge. Additionally, the Cu(I) component must be formed by reduction of either Cu_M(II) or Cu_H(II) by the thiolate of homocysteine in a "sacrificial" reductive process similar to that observed in the metalation of CuA by aqueous $CuSO_4$ where the reduced thiols of the apo protein serve as the source of the reducing electron. [40]

2 Cu(II)-Cu(II)-PHM + 2 S-Pep ⟶ *2 Cu(II)-Cu(I)-PHM + Pep-S-S-Pep* … (2)

2 Cu(II)-Cu(I)-PHM + 2 S-Pep ⟶ *2Cu(II)-S-pep-Cu(I)-PHM (MV spectrum)* … (3)

With an overall reaction:

Cu(II)-Cu(II)-PHM + 2 S-Pep ⟶ *Cu(II)-S-pep-Cu(I) + ½ Pep-S-S-Pep* … (4)

This mechanism predicts that 2 equivalents of peptide are required to elicit the full mixed valence spectrum close to what is observed. Finally, in the S-peptide, EPR data suggested that even when the MV appeared to be fully formed with no further increase in UV-vis intensity on peptide addition, only ~60 percent of the total PHM had been converted. This observation could be rationalized if the peptide disulfide could compete with peptide thiol for binding to oxidized PHM, via the carboxy-terminal peptide binding at residues R240 and Y318.

This chemistry formed the basis for exploration of the reactivity of AAF-hSeCys with oxidized PHM. Figure 5(a) compares the S- and Se-peptide MV spectra for equimolar (600 μM enzyme, 1.2 mM Cu) PHM samples, where the latter was generated by reaction of 2.5 equivalents of the AAF-hSeCys with the oxidized enzyme. (The S-peptide data was generated using the N-Acetyl-AAF-hCys which gave maxima at 450, 570 and 920 nm, blue shifted ~10 nm from that reported for the unmodified N-terminus). Significant differences exist between S- and Se spectra (λ_{max} (Se) = 350, 475, 560 and 1000 nm), most notable the 80 nm red-shift in the NIR band. A control reaction with the AAF-SeMet peptide (Figure S4) did not lead to evolution of any bands in the 800 – 1100 nm region attributable to a mixed valence species, although some minor spectral changes in the d-d region suggested that binding of the peptide had occurred.

EXAFS of the mixed valence species at the Cu edge. EXAFS of the AAF-hSeCys MV species was measured at the Cu edge only, since the excess Se in the sample rendered the Se edge data difficult to interpret. Cu K-EXAFS of the AAF-hSeCys complexes with oxidized PHM is shown in Fig. 5(c) with parameters listed in Table 1. Best fit simulations give 2.5 Cu-N(His), 0.5 Cu-S(Met314) and 0.7 Cu-Se(hCys) with bond lengths of 1.95, 2.20, and 2.41 Å respectively. The substoichiometric occupation number for the Cu-Se shell is consistent with ~70 percent formation of the Se bridged species, with the remaining oxidized enzyme bound by the diselenide peptide (*vide supra*). The Cu-S(Met314) interaction is notably shorter than typically found in the WT PHM possibly the result of a stronger interaction of the Se with the reduced CuH center, allowing a stronger interaction with the S(Met314) ligand. Comparison of MV and fully reduced PHM-AAF-hSeCys absorption edges (Figure 5(d)) shows the expected shift to lower energy for the reduced state, and a weak partially resolved 1s –> 3d quadrupole transition from the Cu(II) components in the MV complex at 8979 eV. These absorption edges are unremarkable but are shown here for completeness.

EPR Analysis of the AAF-hSeCys mixed-valence complex. EPR spectra for the oxidized PHM starting material and its MV complex generated from titration with the reduced selenopeptide are shown in Figure 6(a) and (b) respectively. For each sample, the quantity of Cu(II) represented by the EPR intensity was determined by double integration relative to a Cu(II)-EDTA standard measured under identical experimental conditions of microwave power, modulation amplitude, and temperature. The amount of EPR detectable Cu(II) is correlated with the absorbance maximum at 1000 nm in Table S2. Spectra were simulated using Easyspin[41] and the simulations are shown as red traces in Figure 6 with parameters used in the simulations in Table S3.

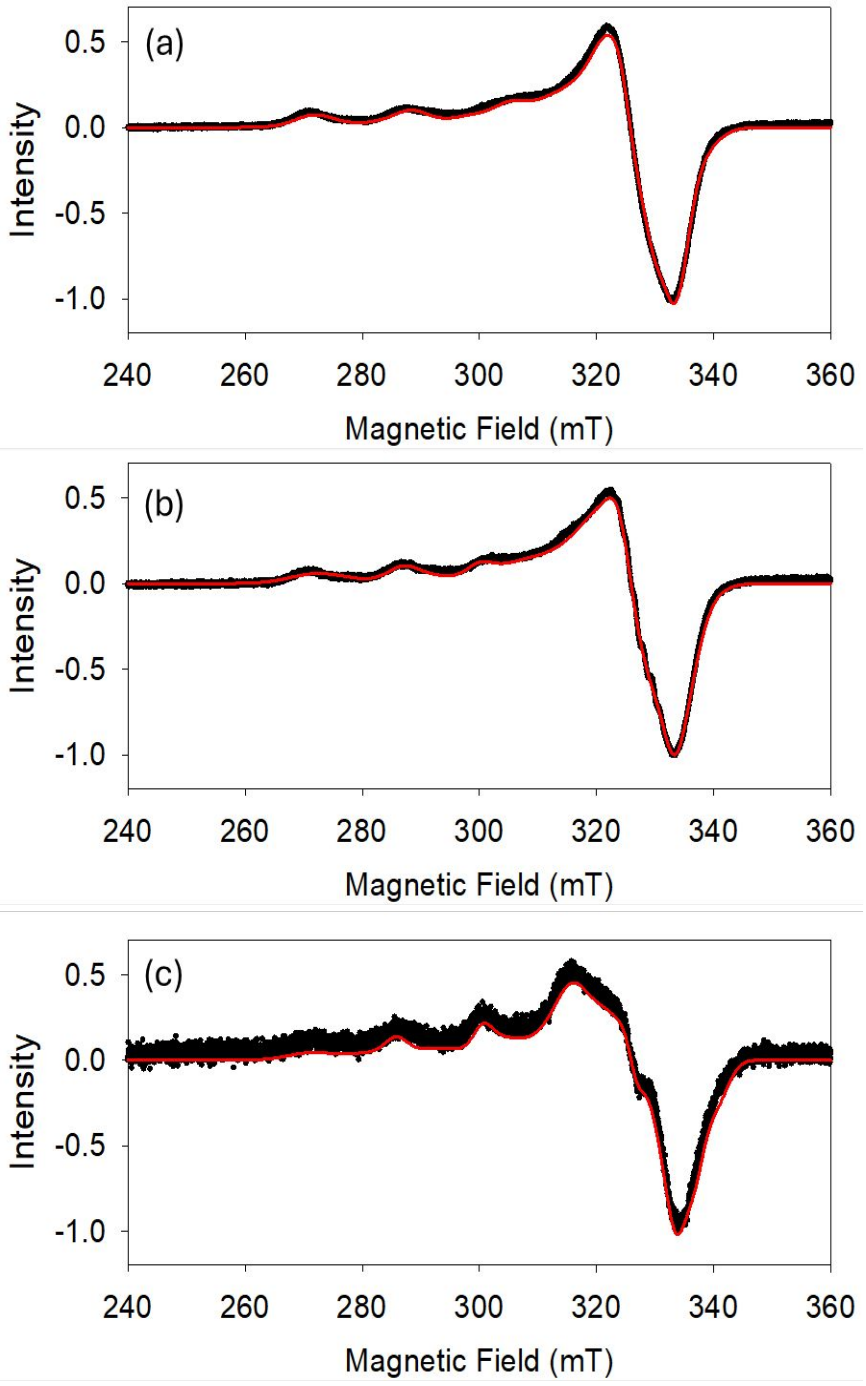

Figure 6. EPR spectra (black traces) of oxidized PHM and its reaction products with the AAF-hSeCys peptide. (a) unreacted oxidized PHM (b) reacted with 2.5 equivalents of AAF-hSeCys (c) after reduction with 5 mM ascorbate. Simulated spectra (red traces) were generated using EASYSPIN (see text). Reaction conditions, concentrations and residual Cu(II) quantitation are listed in Table S2. Parameters used in the fits are listed in Table S3. EPR instrumental conditions were as follows: frequency 9.396 GHz, modulation amplitude 2 Gauss, microwave power 2 mW, temperature 170 K. Spectra are averages of 4 scans each.

Oxidized PHM was found to integrate to 100 percent Cu(II) as expected. The MV

complex integrated to 69 percent Cu(II) and 31 percent of an EPR indetectable form (by subtraction). If we assume that this indetectable copper is Cu(I) we may conclude that 62 percent of the total copper is present as the MV form and 38 percent as a different oxidized form. This latter form cannot be unreacted oxidized PHM since the titration proceeded to an end point where no more selenol would react. The most likely assignment for this species is a diselenide-bound state of the oxidized enzyme where the C-terminal carboxylate of a diselenide form of the peptide competes with the carboxy terminus of the reduced selenol form for the peptidyl binding site. The quantitative EPR analysis would predict that the Cu EXAFS of the titration end point should show ~0.6 Se scatterers per Cu in good agreement with the EXAFS value of 0.7.

Both visual inspection and simulation of the MV species fail to reveal evidence of a 7-line hyperfine pattern expected for a class III MV species exhibiting complete electron delocalization over both copper nuclei. Therefore, we conclude that like its S analogue, the AAF-hSeCys forms a class II localized MV entity where the rate of electron exchange between the two redox states of Cu in the Se-bridged dicopper species is slow relative to the EPR time scale at the temperature of measurement (170 K). It is possible that electron delocalization can occur at room temperature, but RT EPR measurements were of insufficient signal-to-noise to address this question. It is likely that the chemical inequivalence of the two Cu centers in PHM leads to valence localization at low temperature, as was also concluded for the AAF-hCys system.

Reduction of MV complexes by ascorbate. In our earlier work on the AAF-hCys PHM system we observed that the sulfur-bridged MV complex was remarkably resistant to ascorbate reduction and was reduced in a biphasic reaction

$$Abs_{925nm} = A_1 e^{-k_1 t} + A_2 e^{-k_2 t} + A_0 \quad \text{... (5)}$$

with parameters k_1 = 0.09 min^{-1}, and k_2 = 0.007 min^{-1} in a 1:4 ratio. [26] Like the Se system, the S-bridged complex was formed with an accompanying fully oxidized component, but because the latter was reduced much faster by ascorbate than the MV complex, it could be rendered EPR undetectable by reduction with 5 mM ascorbate allowing the EPR spectrum of the MV complex to be visualized without overlap from any additional EPR active species. Despite this, simulation of the S-bridged MV complex required contributions from two S=1/2 species in a 1:3 ratio. The structural and/or electronic differences between these two MV species were not explored but because of the slow electron exchange suggested by their class II MV character one may speculate that they could represent redox states with the unpaired electron localized or "frozen out" onto each of the CuH and CuM sites.

We carried out a similar reaction with the Se-bridged MV system with the expectation that the EPR spectrum of the MV entity could be isolated by similar differential reduction of the accompanying fully oxidized component. This experiment was only partially successful since the Se-containing MV complex appeared to be reduced much more rapidly (Figure 5 (b)) this time in a single exponential with k_{obs}= 0.1 ± 0.01 min^{-1}. However, comparison with the S data indicates that this rate is close to the faster rate observed in the former but is now the major/only component rather than the minor component of the reaction. Given this faster reduction the ascorbate-reduced MV species had undergone significant reduction itself before it could be frozen for EPR analysis. Figure 6(c) shows the EPR spectrum of this species along with its simulation, with EPR parameters listed in Table S3.

The spectra shown in Figure 6 each required at least 2 separate S=1/2 components to obtain satisfactory residuals. For oxidized PHM and the MV complex this is expected since (i) oxidized PHM (Fig. 6(a)) contains two chemically inequivalent copper centers, CuH and CuM and (ii) the MV complex (Fig. 6(b)) contains a residual oxidized component and a MV component with respective Cu(II) concentrations in 4:3 proportions. A 2-component simulation

for the ascorbate-reduced MV system is consistent with the result found for the S-analogue, although the single-phase reductive kinetics are more consistent with a single species. Inspection of the EPR parameters for the MV complexes indicates that the species responsible are unremarkable with g and A values consistent with isolated S=1/2 systems in close-to-axial symmetry, typical of type II rather than type 1 Cu proteins. In particular, the covalency of the Se MV complex appears less than its S analogue where the g_3 -values of both components are in the 2.26 -2.30 region, in contrast to the S-bridged system where g_3 = 2.21 for the major component.

Calculation of the Extinction Coefficient for the MV complex. The extinction coefficient for the IVCT band of the mixed-valence complex was calculated as follows. For samples taken at the titration end-point before any ascorbate reduction, the difference between the total copper concentration and the Cu(II) component derived from the EPR detectable copper was presumed to be the Cu(I) component of the mixed valence complex. For the sample analyzed after ascorbate reduction, the EPR sample was thawed, the OD at 1000 nm measured, and the concentration of EPR detectable copper was now used as the concentration of MV complex, since ascorbate was deemed to have reduced all of the Cu(II) not contained in the MV. These calculations led to 3 independent measurements of the MV extinction coefficient (per protein) as shown in Table S2 which average to 516 ± 16 $M^{-1}cm^{-1}$.

Discussion

Understanding the mechanism of copper monooxygenase such as PHM and DBM has been a topic of intense interest in the field of copper biochemistry, and more broadly in the biomedical community since these enzymes catalyze pharmacologically important processes. Based on an accumulation of evidence, we and others have advanced the idea that the mechanism proceeds via an "open-to-closed" conformational gate that allows the resting mononuclear copper state (Cu-Cu= 10 – 14 Å) to transition to a binuclear copper state (Cu-Cu = 4- 5 Å) induced by some structural or chemical event along the reaction coordinate. In a previous report, we suggested that the open to closed transition might be induced by binding of the anionic substrate to the protonated R240 residue coupled to reduction of the two Cu(II) centers to Cu(I), a process that reduces the net charge in the active site pocket from +5 to +2, and thereby significantly diminishes the electrostatic repulsion between the H and M subdomains. The existence of structures of closed conformers of both PHM and DBM, albeit of only partial copper occupancy, together with supporting evidence from QM/MM calculations that the open-to-closed mechanism is energetically feasible, and indeed that subdomain closure costs a mere 2 kcals mol^{-1}, has spurred efforts to develop approaches to the isolation and characterization of binuclear states that retain their full complement of copper and that can be studied spectroscopically.

Recently we reported the discovery of a binuclear state of PHM in complex with the peptidyl inhibitor AAF-hCys where we proposed that the inhibitor binds in a bifunctional fashion, with the C-terminal carboxylate occupying the usual peptidyl binding site at R240 and Y318, and the thiol from homocysteine coordinating copper, and bridging between the CuM and CuH sites. The evidence for bridging was derived from the Cu K-EXAFS of the ascorbate-reduced forms which required a Cu-S shell occupancy of 1.5 in the native enzyme which dropped to 1S per Cu in the M314H variant where the M-site coordinating methionine was absent. An additional

feature of the AAF-hCys-bound system was the formation of an unusual and extremely stable mixed-valence species when the inhibitor reacted with the fully oxidized enzyme. Since a MV intermediate had been proposed as the initiator of hydrogen atom abstraction (HAT) chemistry in Wang's QM/MM study, observation of a stable MV entity carried additional significance.

In the present study we extended these studies to provide unambiguous evidence for the binuclear state. Substitution of the thiol of homocysteine with selenol provided an additional spectroscopic window via the ability to probe the Se-Cu interactions at both the Cu and the Se X-ray absorption edges. After solving the challenging issue of diselenide reduction, we were successful in forming the AAF-hSeCys-PHM complex in both the fully reduced and mixed-valence states. The fully reduced derivative gave conclusive evidence for the Se bridge between the two coppers where the Se EXAFS data gave a Se-Cu shell occupancy of 1.8, twice that of the Cu-Se shell occupancy (0.85) measured at the Cu edge. Of particular importance, the metrical parameters and DW factors were exactly mirrored at each absorption edge, as required for validation of the chemical model. Our results showed that stoichiometric addition of peptide led to ~90% formation of the bridged species.

The AAF-hSeCys peptide was also able to form the mixed valence species, giving rise to a UV-vis absorption spectrum with a red-shifted NIR band, but similar higher energy features. Red shifted Se-Cu(II) CT bands have been observed in a SeCys analogue of azurin [42, 43] suggesting that the more reducing Cu(II)-Se interaction lowers the energy of the half-filled LUMO, and/or stabilizes the transient Cu(I) species in the excited state. Studies on selenium and sulfur Cu(I) biomimetic complexes[44, 45] have also demonstrated a strong decrease in redox potential (increased reducing power) and strong stabilization of Cu(I) by the selenium ligand. However, any analysis of the UV-vis data for this apparent MV complex must make assumptions as to which of the two Cu centers (H or M) is reduced and which remains oxidized. In the absence of bound substrate, the M-site redox potential is more negative by 285 mV,

although the two potentials equalize at +83 mV when the substrate Ac-YVG is bound.[46] This may suggest that the M-center is more favorable for Cu(II) binding, and when coordinated by a chalcogenide ligand would exhibit a "cupredoxin-like" His_2-Met-S/Se(Cys) ligand set, which has been described in terms of the coupled distortion model.[47, 48].

Cupredoxins such as plastocyanin and azurin have distorted tetrahedral symmetry with the Cu(II) center coordinated by 2 His and one Cys residue in roughly trigonal arrangement and a long weak axial interaction with the thioether of a methionine residue. These classic "blue" or type I copper proteins exhibit intense low energy (~600 nm) S(p_π) to Cu(II) charge transfer absorption bands and short Cu-S distances (2.07 – 2.15 Å) associated with the strong covalency of their $d_{x^2-y^2}$ to S-p π-bond. A weaker band assigned as a S(p_σ) to Cu(II) CT is observed around 400 nm[49, 50]. As the protein structures across the cupredoxin family are perturbed the coordination geometry of the copper center distorts such that the overlap between the Cu(II) d(x^2-y^2) and the S(p_σ) increases while that with the Sp($_\pi$) weakens and loses intensity. The distortion causes the interaction with the axial ligand to increase, and In the limit of a strong axial interaction a 5-coordinate distorted square pyramidal site is formed of the type found in the "red" copper proteins nitrosocyanin[51, 52] and Sco [53]. The latter exhibit normal Cu-S distances around 2.25 Å and dominant higher energy LMCT bands between 350 and 400 nm due to ligand-σ to Cu(II) charge transfer[53, 54]. Green copper proteins such as nitrite reductase have intermediate LMCT behavior where weakened Sp($_\pi$) together with lower energy ligand-σ interactions result in two bands of almost equal intensity between 460 and 500 nm[48]. However, while the coupled distortion model is an excellent basis for discussing cupric thiolate and selenolate electronic spectra, significant diversity exists within the family, a notable example being the "green" center of AcoP from *Acidithiobacillus ferrooxidans* where a long Cu-S(cys) bond of 2.23 Å is not compensated by a shortened axial Cu-S(Met) bond [55].

The electronic absorption spectra of the sulfur-containing AAF-hCys complexes of PHM shows very similar properties to that of AcoP while EXAFS gives a long Cu-S distance (2.25 Å) accompanied by uncompensated long Cu-S(Met) distances. [26] The Se complex, on the other hand, while showing a normal Cu-Se bond (2.39 Å), appears to have a compensatory short Cu-S(Met) bond (2.20 Å). This could be due to different degrees of ligand set distortion arising from the thiolate versus the selenolate coordination, perhaps as the result of varying interaction of the chalcogenide with the Cu(I) component of the ligand bridge. This interpretation is reasonable in light of the anticipated stronger Cu(I) selenolate interaction.

While not yet validated experimentally, the binuclear formulation explains experimental data that are poorly accounted for in the mononuclear mechanism. First, contrary to expectation from model studies in organic solvents at low-temperature,[56-65] O_2 appears unreactive towards *water soluble* mononuclear M-site protein analogues engineered into the small metallochaperone scaffold CusF.[66] Both Cu(II) and Cu(I) derivatives could be formed by simple reconstitution with either aqueous Cu(II) or Cu(I)-acetonitrile, and these faithfully reproduced the spectroscopy of the WT, CO- and azide-complexes of the PHM M-site. To test the oxygen reactivity we exposed the Cu(I) complex to air in the presence of sodium azide and monitored the appearance of any Cu(II)-azido species at 390 nm but observed no reaction over a period of 24 h. If O_2 reacted with the mononuclear Cu(I)His_2Met ligand set to form a Cu(II)-superoxo, azide should displace the $O_2^{-\bullet}$ which would then rapidly disproportionate in aqueous solution to O_2 and H_2O_2 leading to full formation of the Cu(II)-azido complex.

A second compelling line of evidence in favor of a binuclear intermediate stems from peroxide shunt chemistry.[67] In earlier work we reported that product could be formed catalytically from oxidized PHM and hydrogen peroxide, but when $H_2{}^{18}O_2$ was used as the source of O in the product the hydroxylated isomer contained 60 percent ^{16}O due to exchange with ambient molecular oxygen. Solvent was eliminated as the origin of the ^{16}O by testing the

reaction of $H_2{}^{16}O_2$ in D_2O where no exchange was observed. Under strictly anaerobic conditions, product formation and peroxide consumption were tightly coupled, and the rate of product formation was identical to that measured under aerobic conditions. The result required the reaction to cycle through an intermediate where a Cu(II)-peroxide or hydroperoxide is in equilibrium with a Cu(I) dioxygen species. The simplest explanation for this chemistry would be a species similar to that of the well characterized binuclear copper centers of hemocyanin and tyrosinase, [68-70] but at the time we were reluctant to propose such an entity in PHM since there was no evidence for any closed conformations. Instead we proposed that peroxide first reduced CuH generating Cu(I)H and superoxide, and the latter then channeled across the 11 Å solvent-filled cleft where it bound as the Cu(II)M superoxo species which was theoretically in equilibrium with Cu(I)-dioxygen. In retrospect, this mechanism has serious flaws; (i) it requires peroxide to act as both a reductant and oxidant under the same conditions, (ii) crystallography has shown that peroxide binds only at CuM[71] and (iii) superoxide should leak from the site leading to uncoupling of peroxide consumption from product formation. Therefore, access to a binuclear state via a closed conformation seems a more plausible explanation.

A third observation not readily accommodated by the canonical mechanism derives from kinetic isotope studies on the H172A variant. Removal of a CuH ligand might be expected to reduce ET rates from H to M and indeed the mutation lowered rates of electron transfer 400 - 2000 fold. However, a much larger effect was observed for the H atom abstraction (HAA) step where the rate was reduced by a factor of 12000 relative to WT. This implies that H172A has a large influence on the energy and/or dynamics required to form the transition state within which HAA chemistry can proceed. While this might involve solvent-induced reorganization of H-bonding pathways or global conformational effects that perturb the structure of the ES complex, the magnitude of the effect suggests direct structural involvement of this ligand in the transition state.

Other data underscore the requirement for substrate triggering of catalysis via induction of an active state such as the closed conformer. Substrate binding is always completely coupled to product hydroxylation even with slow substrates and/or slow variants establishing that substrate activation is required to generate the catalytically active species.[2, 13, 72] Furthermore, structural evidence for substrate-induced perturbation of CuM electronic and/or geometric structure is well-documented from CO reactivity where the CO stretching frequency for CuM-CO complex is red shifted by 30 cm^{-1} in the presence of the substrate Ac-YVG. It has been suggested that this shift may be due to formation of a bridging or semi-bridging mode previously attributed to homo- or hetero-bimetallic systems[2, 11, 73, 74].

The stability of the MV complexes is remarkable where both S- and Se- complexes are stable for hours at room temperature. In the presence of reducing agents (5 mM ascorbate) both complexes undergo slow bleaching due to reduction of the Cu(II) component. As mentioned above, the recent QM/MM study invoking the open-to-closed mechanism has predicted a MV complex with a bridging peroxo ligand as an energetically feasible intermediate for H atom abstraction from the substrate C-alpha. The inherent stability of the PHM active site in a MV form adds experimental validation to this premise, since active sites built to accommodate MV species are rare, unless they are mechanistically relevant. We may speculate that in the absence of an exogenous bifunctional reagent such as AAF-hCys, a viable path to a *catalytic* MV intermediate would be an imidazole bridge formed by sharing of a His residue between both Cu centers. H-site ligand H172 is a good candidate for this role, since *vide supra*, this His must play an essential role in the structural organization of the chemical intermediate.[14] Other candidates include hitherto unidentified protein side groups or hydroxide from solvent. Further studies using C-terminal histidine- and threonine containing tetrapeptides are underway to test these possibilities.

Materials and Methods

Materials. All materials were of reagent grade and were purchased from Sigma-Aldrich unless stated otherwise. Peptidylglycine monooxygenase catalytic core (residues 42 – 356) was produced from recombinant chinese hamster ovary cells (CHO) in a Accusyst MiniMax hollow fiber bioreactor (Cell Culture Co., Minneapolis) using methodologies previously described [75, 76]. Enzyme purification, copper reconstitution, and copper to protein analysis were performed as previously described [26, 75, 76]. Protein concentration was determined from the OD_{280} (1%) = 0.985, and copper and selenium concentrations were determined by inductively coupled plasma optical emission (ICPOES) spectrometry on a Perkin Elmer Optima 2000 ICPOES instrument. Enzyme samples used in this work were >95% pure by SDS gel electrophoresis and routinely contained 2.0 ± 0.1 Cu atoms per monomer of 35 kDaltons.

Solid-phase synthesis, purification, and mass spectrometry characterization of the AAF-hSeCys peptide. The AAF-hSeCys and AAF-SeMet peptides were synthesized on a Chorus peptide synthesizer (Protein Technologies Inc.). The synthesis followed standard Fmoc procedures provided by the manufacturer and was carried out on a 0.10 mmol scale. All natural Fmoc-amino acids were purchased from Protein Technologies Inc. Fmoc-hSeCys(pMOB)-OH and Fmoc-L-Selenomethionine were purchased from ChemPep (#350313 and #351303). For the syntheses, 300 mg of 2-chlorotrityl chloride resin 100-200 mesh (ChemPep) was loaded with 0.10 mmol of Fmoc-hSeCys(pMOB)-OH or Fmoc-L-Selenomethionine. The resin was washed three times with 5 mL N,N-dimethylformamide (DMF) and three times with 5 mL dichloromethane (DCM). Each respective Fmoc amino acid (AA) was dissolved in 1 mL of 1:1 DCM with 0.15 mmol diisopropylethylamine (DIPEA). This solution was added to the resin and gently shaken for 1 hour. The Fmoc-AA/DIPEA solution was then drained from the resin, and the resin was washed three times with 5 mL of DCM. The uncapped sites on the resin were capped by washing with 20 mL of 17:2:1 DCM:methanol. The resin was then washed three

times with 5 mL of DCM and three times with 5 mL of DMF. The resin was then transferred to the reaction vessel.

All Fmoc-amino acids (0.60 mmol, 6 equivalents) were coupled by in situ activation with (1-[bis(dimethylamino)methylene]-1H-1,2,3-triazolo[4,5-b]pyridinium 3-oxide hexafluorophosphate (HATU) (0.60 mmol, 6 equivalents; ChemPep) in 0.6 M N-methylmorpholine. The AAF-hSeCys peptide was deprotected and cleaved from the resin in a solution containing 96% (v/v) trifluoroacetic acid (TFA), 2% (v/v) water (H_2O), and 2% (v/v) triisopropylsilane (TIS). 5mL of the cleavage buffer was added to the resin and the slurry was stirred at 50 °C for 4 hours. The cleavage reaction was filtered into 30 mL of ice-cold diethyl ether to precipitate the peptide. The solution was centrifuged at 11,000 x g for 3 minutes and the supernatant was decanted. The remaining residue was re-suspended in 30 mL of ice-cold diethyl ether and centrifuged again at 11,000 x g for 3 minutes. The supernatant was decanted once more, and the remaining residue was placed under a slow-flow nitrogen line for 10 minutes to evaporate any residual diethyl ether. The remaining peptide residue was re-suspended in 20 mL of water, flash frozen in liquid nitrogen, and lyophilized. The AAF-SeMet peptide underwent the same process but was cleaved for 2 h at RT instead.

The peptides were purified using high-performance liquid chromatography (HPLC) with a Phenomenex Jupiter C18 preparative column (21.2 mm x 250 mm, 5 µm particle size, 300Å pore size) with buffer A as 0.1% trifluoroacetic acid (TFA, HPLC grade) in nanopure water and buffer B as 0.1% TFA (HPLC grade) in acetonitrile (ACN, HPLC grade). The separation used a flow rate of 5 mL/min with a linear gradient of buffer A from 88% to 55% over 70 minutes. The deprotected diselenide peptide eluted at 49 minutes under these conditions and the AAF-SeMet peptide eluted at 44 minutes. Fractions were analyzed by LC-MS using a HPLC-HRMS setup (Vanquish UHPLC with a diode array detector connected to a Q-Exactive) fitted with a Hypersil GOLD C18 column (2.1 mm x 150 mm, 1.9 µm particle size) for separations at 0.2 mL/min. The

LC-MS program for peptide fraction identification was set up as follows: buffer A was LC-MS Optima water (Fisher)/0.1% (v/v) LC-MS Optima TFA (Fisher) and buffer B was LC-MS Optima ACN (Fisher)/0.1% (v/v) LC-MS Optima TFA (Fisher). The 15-minute separation consisted of washing the column with 100% A for 3 minutes, followed by a linear gradient to 100% B from 3 to 6 minutes, followed by washing the column with 100% B from 6 to 9 minutes, a decreased gradient from 100% B to 0% B over 9 to 12 minutes, and finally re-equilibration in 100% A from 12 to 15 minutes. The MS detectors operated in positive ion mode, and the FT analyzer settings were as follows: 70,000 resolution, 1 microscan, and 200 ms maximum injection time. MS data analysis used Xcalibur software (Thermo Fisher). Mass spectra of the peptide products are reported in Figure S1.

Inhibitory effects of reductants on PHM activity. To determine if DTT and borohydride interfered with enzyme activity an oxygen consumption experiment was performed using a Rank Brother oxygen electrode as previously described.[25] Similar procedures were used to test the inhibitory effect of DTT and $NaBH_4$. For $NaBH_4$ three separate reactions were performed, each in 2 ml of buffered solution (50 mM MES pH 5.5, 30 mg/ml catalase, 25 μM $CuSO_4$, 100 μM acetyl-YVG substrate) with 1 μM PHM. Reactions were initiated by adding 10 μl of 2 M ascorbate. In the first reaction, normal enzyme activity was assessed with no additional additives, resulting in complete deoxygenation of the buffer over the course of approximately 5 minutes. In the second experiment, after approximately half the oxygen was consumed a small volume of concentrated $NaBH_4$ in DMSO was added to a final concentration of 50 μM. The reaction was instantly arrested, accompanied by the formation of hydrogen gas. In the final reaction, after approximately half the oxygen was consumed a small volume of concentrated borohydride in DMSO quenched with 1 molar equivalent of TFA was added to a final concentration of 50 uM, resulting in no decrease in catalytic rate.

Generation of TFA quenched, borohydride reduced, AAF-hSeCys peptide. 50 µl of 50 mM AAF-hSeCys peptide in anhydrous anaerobic DMSO was thawed in a Vacuum Atmospheres anaerobic chamber (oxygen < 1 PPM). Peptide was reduced by adding 1 M $NaBH_4$ in DMSO to a final concentration of 250 mM (5 molar equivalents), which resulted in rapid evolution of hydrogen gas. The solution was allowed to react for 30 minutes after which the remaining excess borohydride was quenched via the addition of 250 mM TFA (1 molar equivalent per initial borohydride concentration), again resulting in rapid evolution of gas. After 5 minutes another 0.2 molar equivalents of TFA was added resulting in no further effervescence. The solution of TFA quenched AAF-hSeCys peptide was then transferred to a septum-sealed vial for use in further experiments.

XAS sample preparation of AAF-hSeCys peptide with borohydride. 50 µl of 50 mM AAF-hSeCys peptide in anhydrous anaerobic DMSO was thawed in the anaerobic chamber as above and used to make a 2 mM stock solution in 50 mM sodium phosphate buffer pH 7.5 with 20% ethylene glycol as a cryoprotectant. Samples reduced with 1 molar equivalent (2 mM) borohydride, 5 molar equivalents (10 mM), and 5 molar equivalents followed by a TFA quench were prepared as above and transferred to EXAFS cuvettes. The samples were frozen by rapid immersion in liquid nitrogen and stored under liquid N_2 before loading into cassettes at the beam line.

XAS sample preparation of reduced PHM with AAF-hSeCys peptide. 900 uM PHM (1.8 mM in Cu) in 50 mM sodium phosphate buffer pH 7.5 was brought into the anaerobic chamber and allowed to degas exhaustively overnight. Once degassed the PHM solution was reduced via the addition of 5 mM sodium ascorbate, resulting in an immediate color change from blue to clear. Parallel to this, TFA-quenched AAF-hSeCys peptide was prepared using the protocol described above. Two 100 µl samples of 900 µM PHM with either 1 or 2 molar equivalents per protein of AAF-hSeCys peptide were prepared in 50 mM sodium phosphate pH 7.5 with 20% ethylene

glycol. For the 1:2 sample any excess peptide was then removed using spin-desalting columns pre-equilibrated with 50 mM sodium phosphate pH 7.5, 5 mM ascorbate and 20% ethylene glycol. All samples were loaded into XAS cuvettes, flash frozen in liquid nitrogen, and stored under liquid nitrogen until data collection.

Titration of oxidized PHM with TFA-quenched AAF-hSeCys peptide. UV-vis spectra were collected on a Varian Cary 50 UV-vis spectrophotometer between 300 and 1100 nm. A 1 ml solution of 600 μM oxidized PHM (1.2 mM Cu) in 100 mM sodium phosphate buffer pH 7.5 was transferred to a quartz cuvette. Aliquots of 0.5 molar equivalents of anaerobic TFA-quenched reduced AAF-hSeCys were added via syringe and mixed by inverting the cuvette. During the titration the solution turned from blue to deep purple. In some experiments, precipitation was observed, and these samples were spun at 10000 x g for 2 minutes to clarify the solution. Spectra were measured immediately after mixing and again after 5 minutes at a scan rate of 1200 nm/min. Aliquots of peptide were added until no further increase at 1000 nm was observed.

Reduction of the mixed valence complex by ascorbate. Reduction kinetics of the purple MV species were assessed after the titration had reached a maximum absorbance. 2 M stock sodium ascorbate was added to a final concentration of 5 mM and mixed by gentle inversion of the cuvette. Spectra were collected every 5 minutes for 2 hours, then every hour for the next 24 hours.

EPR of oxidized PHM, mixed valence, and ascorbate-reduced mixed valence species. 300 μl of oxidized PHM (600 uM, 1.2 mM in Cu) was frozen in a quartz EPR tube. Further EPR samples were derived from the UV-vis titration to ensure comparability. After the final addition of AAF-hSeCys peptide, 300 μl of this solution was transferred to an EPR tube. Immediately after the addition of 5 mM ascorbate another 300 μl was removed and placed in a EPR tube and frozen as quickly as possible (approximately 3 minutes) to minimize reduction of the MV

species. A final 300 µl was removed after 24 hours of reduction and placed in a EPR tube. EPR data were collected on a Bruker E500 X-Band EPR spectrometer with a liquid nitrogen cryostat. Spectra are averages of 4 scans and collected at a frequency of 9.396 GHz, 170K temperature, 2 mW microwave power, and 2 gauss modulation amplitude. Spectra at higher powers and different modulation amplitudes were also measured to check for power saturation and/or modulation broadening (not observed). Experimental data were simulated using EasySpin. [41]

Titration of oxidized PHM with AAF-SeMet and reduction with ascorbate. UV-vis spectra were collected similarly as above. 1 ml of 600 uM oxidized PHM (1.2 mM Cu) in 100 mM sodium phosphate buffer pH 7.5 was transferred to a quartz cuvette. Aliquots of AAF-SeMet peptide in 50% methanol, 50% 100 mM sodium phosphate buffer were added, then mixed by inversion of the cuvette. Slight cloudiness was observed and removed by spinning at 10000 x g for 2 minutes. Spectra were taken immediately and after 5 minutes at a scan rate of 1200 nm/min. Aliquots were added up to 5 molar equivalents which elicited only minor perturbation of the oxidized PHM spectrum. The spectra are shown in Figure S4.

After the titration to 5 molar equivalents, 600 µM sodium ascorbate was added to assess if the addition of one molar equivalent per copper of a reducing agent could induce the formation of a mixed valence complex. This reaction resulted in decrease in the 650 nm Cu(II) d-d band but did not elicit any bands in the MV region.

Author Information

Corresponding Author

*§ Ninian J. Blackburn, Department of Chemical Physiology and Biochemistry, Oregon Health & Science University, Portland, OR 97239 USA

ORCID**:** 0000-0002-9755-7838

blackbni@ohsu.edu

Authors

§ Evan F. Welch, Department of Chemical Physiology and Biochemistry, Oregon Health & Science University, Portland, OR 97239 USA.

† Katherine W. Rush, Department of Chemistry and Biochemistry, Auburn University, Auburn, AL 36849 USA; ORCID:0000-0002-2754-4222

‡ Karsten A.S. Eastman, Department of Chemistry, University of Utah, Salt Lake City, UT 84112, USA; orcid.org/0000-0002-2754-4222

‡ Vahe Bandarian, Department of Chemistry, University of Utah, Salt Lake City, UT 84112, USA; orcid.org/0000-0003-2302-0277

Funding Sources: This work was supported by NIGMS 1R35GM136239 (to N.J.B.), NIGMS R35GM126956 (to V.B.), and NIH T32-GM122740 (to K.A.S.E.).

Author Contributions. Experimental design was conceived jointly by EFW, VB and NJB. KASE synthesized and purified the homoselenocysteinyl and selenomethionyl peptides. KWR and EFW contributed equally to data collection and analysis. The manuscript was written jointly by EFW, KASE, and NJB.

Conflicts of Interest

There are no conflicts to declare.

Data Availability. The data supporting this article are included as Figures and Tables either in the main article or as Supplementary Information.

ACKNOWLEDGMENT

Use of the Stanford Synchrotron Radiation Lightsource, SLAC National Accelerator Laboratory, is supported by the U.S. Department of Energy (DOE), Office of Science, Office of Basic Energy Sciences under Contract No. DE-AC02-76SF00515. The SSRL Structural Molecular Biology Program is supported by the DOE Office of Biological and Environmental Research, and by the National Institutes of Health, National Institute of General Medical Sciences (P30GM133894). The authors would like to thank Tamar Conner for assistance with cell growth and protein purification.

References

1. D. J. Merkler, A. J. Hawley, B. A. Eipper and R. E. Mains, *Br. J. Pharmacol.*, 2022, **179**, 3306-3324.
2. E. F. Welch, K. W. Rush, R. J. Arias and N. J. Blackburn, *J Inorg Biochem*, 2022, **231**, 111780.
3. J. P. Klinman, *J. Biol. Chem.*, 2006, **281**, 3013-3016.
4. C. R. Hess, M. M. McGuirl and J. P. Klinman, *J. Biol. Chem.*, 2008, **283**, 3042-3049.
5. S. T. Prigge, R. E. Mains, B. A. Eipper and L. M. Amzel, *Cell. Mol. Life Sci.*, 2000, **57**, 1236-1259.
6. T. V. Vendelboe, P. Harris, Y. Zhao, T. S. Walter, K. Harlos, K. El Omari and H. E. Christensen, *Sci. Adv.*, 2016, **2**, E1500980.
7. L. S. Mydy, J. Hungerford, D. N. Chigumba, J. R. Konwerski, S. C. Jantzi, D. Wang, J. L. Smith and R. D. Kersten, *Nat Chem Biol*, 2024, **20**, 530-540.
8. N. J. Blackburn, F. C. Rhames, M. Ralle and S. Jaron, *Journal of Biological Inorganic Chemistry*, 2000, **5**, 341–353.
9. J. S. Boswell, B. J. Reedy, R. Kulathila, D. J. Merkler and N. J. Blackburn, *Biochemistry*, 1996, **35**, 12241-12250.
10. P. Chen, J. Bell, B. A. Eipper and E. I. Solomon, *Biochemistry*, 2004, **43**, 5735-5747.
11. S. Jaron and N. J. Blackburn, *Biochemistry*, 1999, **38**, 15086-15096.
12. V. Martin-Diaconescu, K. N. Chacon, M. U. Delgado-Jaime, D. Sokaras, T. C. Weng, S. DeBeer and N. J. Blackburn, *Inorg. Chem.*, 2016, **55**, 3431-3439.
13. J. P. Evans, K. Ahn and J. P. Klinman, *J. Biol. Chem.*, 2003, **278**, 49691-49698.
14. J. P. Evans, N. J. Blackburn and J. P. Klinman, *Biochemistry*, 2006, **45**, 15419-15429.
15. W. A. Francisco, M. J. Knapp, N. J. Blackburn and J. P. Klinman, *J. Am. Chem. Soc.*, 2002, **124**, 8194 - 8195.

16. W. A. Francisco, D. J. Merkler, N. J. Blackburn and J. P. Klinman, *Biochemistry*, 1998, **37**, 8244-8252.

17. J. P. Klinman, *Chem. Rev.*, 1996, **1996**, 2541-2561.

18. P. Chen and E. I. Solomon, *J. Am. Chem. Soc.*, 2004, **126**, 4991-5000.

19. P. Chen and E. I. Solomon, *Proc. Natl. Acad. Sci. U S A*, 2004, **101**, 13105-13110.

20. R. E. Cowley, L. Tian and E. I. Solomon, *Proc. Natl. Acad. Sci. USA*, 2016, **113**, 12035-12040.

21. A. Crespo, M. A. Marti, A. E. Roitberg, L. M. Amzel and D. A. Estrin, *J. Am. Chem. Soc.*, 2006, **128**, 12817-12828.

22. P. Wu, F. Fan, J. Song, W. Peng, J. Liu, C. Li, Z. Cao and B. Wang, *J. Am. Chem. Soc.*, 2019, **141**, 19776-19789.

23. S. T. Prigge, B. A. Eipper, R. E. Mains and L. M. Amzel, *Science*, 2004, **304**, 864–867.

24. S. Maheshwari, C. Shimokawa, K. Rudzka, C. D. Kline, B. A. Eipper, R. E. Mains, S. B. Gabelli, N. Blackburn and L. M. Amzel, *Commun. Biol. (Nature Publishing)*, 2018, **1**, 74.

25. R. J. Arias, E. F. Welch and N. J. Blackburn, *Protein Science*, 2023, **32**, e4615.

26. K. W. Rush, K. A. S. Eastman, E. F. Welch, V. Bandarian and N. J. Blackburn, *J. Am. Chem. Soc.*, 2024, **146**, 5074-5080.

27. A. N. Barry and N. J. Blackburn, *Biochemistry*, 2008, **49**, 4916-4928.

28. K. B. Alwan, E. F. Welch and N. J. Blackburn, *Biochemistry*, 2019, **58**, 4436-4446.

29. T. D. Westmoreland, D. E. Wilcox, M. J. Baldwin, W. B. Mims and E. I. Solomon, *J . Am. Chem. Soc.*, 1989, **111**, 6106-6123.

30. R. R. Gagne, C. A. Koval, T. J. Smith and M. C. Cimolino, *J. Am. Chem. Soc.*, 1979, **101**, 4571-4580.

31. N. J. Blackburn, M. E. Barr, W. H. Woodruff, J. van der Oost and S. de Vries, *Biochemistry*, 1994, **33**, 10401-10407.

32. N. J. Blackburn, S. de Vries, M. E. Barr, R. P. Houser, W. B. Tolman, D. Sanders and J. A. Fee, *J. Am. Chem. Soc.*, 1997, **119**, 6135-6143.

33. J. A. Farrar, F. Neese, P. Lappalainen, P. M. H. Kroneck, M. Saraste, W. G. Zumft and A. J. Thompson, *J. Am. Chem. Soc.*, 1996, **118**, 11501-11514.

34. P. M. H. Kroneck, *J. Biol. Inorg. Chem.*, 2018, **23**, 27-39.

35. D. R. Gamelin, D. W. Randall, M. T. Hay, R. P. Houser, T. C. Mulder, G. W. Canters, S. de Vries, W. B. Tolman, Y. Lu and E. I. Solomon, *J. Am. Chem. Soc.*, 1998, **120**, 5246-5263.

36. K. R. Williams, D. R. Gamelin, L. B. Lacroix, R. P. Houser, W. B. Tolman, M. C. Mulder, S. de Vries, B. Hedman, K. O. Hodgson and E. I. Solomon, *J. Am. Chem. Soc.*, 1997, **119**, 613-614.

37. R. P. Houser, V. G. J. Young and W. B. Tolman, *J. Am. Chem. Soc.*, 1996, **118**, 2101-2102.

38. M. T. Hay, M. C. Ang, D. R. Gamelin, E. I. Solomon, W. E. Antholine, M. Ralle, N. J. Blackburn, P. D. Massey, X. Wang, A. H. Kwon and Y. Lu, *Inorg. Chem.*, 1998, **37**, 191-198.

39. S. DeBeer George, M. Metz, R. K. Szilagyi, H. Wang, S. P. Cramer, Y. Lu, W. B. Tolman, B. Hedman, K. O. Hodgson and E. I. Solomon, *J. Am. Chem. Soc.*, 2001, **123**, 5757-5767.

40. K. N. Chacon and N. J. Blackburn, *J. Am. Chem. Soc.*, 2012, **134**, 16401-16412.

41. S. Stoll and A. Schweiger, *J. Magn. Reson.* , 2006, **178**, 42-55.

42. S. M. Berry, M. D. Gieslelman, M. J. Nilges, W. A. van der Donk and Y. Lu, *J. Am. Chem. Soc.*, 2002, **124**, 2084-2085.

43. M. Ralle, S. M. Berry, M. J. Nilges, M. D. Gieselman, W. A. van der Donk, Y. Lu and N. J. Blackburn, *J. Am. Chem. Soc.*, 2004, **126**, 7244-7256.

44. M. M. Kimani, J. L. Brumaghim and D. VanDerveer, *Inorg. Chem.*, 2010, **49**, 9200-9211.

45. B. N. Sánchez-Eguía, H. Hernández-Toledo, S. Lidin, M. Flores-Alamo, E. Nordlander, S. Bertaina, M. Orio and I. Castillo, *ChemCatChem*, 2025, **17**, e202401330.

46. S. Chauhan, P. Hosseinzadeh, Y. Lu and N. J. Blackburn, *Biochemistry*, 2016, **55**, 2008-2021.

47. E. I. Solomon, *Inorg. Chem.*, 2006, **45**, 8012-8025.

48. L. B. LaCroix, S. E. Shadle, Y. Wang, B. A. Averill, B. Hedman, K. O. Hodgson and E. I. Solomon, *J. Am. Chem. Soc.*, 1996, **118**, 7755-7768.

49. E. I. Solomon, M. J. Baldwin and M. L. Lowery, *Chem. Rev.*, 1992, 521-542.

50. S. E. Shadle, J. E. Penner-Hahn, H. J. Schugar, B. Hedman, K. O. Hodgson and E. I. Solomon, *J. Am. Chem. Soc.*, 1993, **115**, 767-776.

51. D. M. Arciero, B. S. Pierce, M. P. Hendrich and A. B. Hooper, *Biochemistry*, 2002, **41**, 1703-1709.

52. R. L. Lieberman, D. M. Arciero, A. B. Hooper and A. C. Rosenzweig, *Biochemistry*, 2001, **40**, 5674-5681.

53. G. S. Siluvai, M. Mayfield, M. J. Nilges, S. DeBeer George and N. J. Blackburn, *J. Am. Chem. Soc.*, 2010, **132**, 5215-5226.

54. L. Andruzzi, M. Nakano, M. J. Nilges and N. J. Blackburn, *J. Am. Chem. Soc*, 2005, **127**, 16548-16558.

55. M. Roger, P. Leone, N. J. Blackburn, S. Horrell, T. M. Chicano, F. Biaso, M. T. Giudici-Orticoni, L. A. Abriata, G. L. Hura, M. A. Hough, G. Sciara and M. Ilbert, *Dalton Trans*, 2024, **53**, 1794-1808.

56. P. Chen, D. E. Root, C. Campochiaro, K. Fujisawa and E. I. Solomon, *J. Am. Chem. Soc.*, 2003, **125**, 466-474.

57. R. L. Peterson, J. W. Ginsbach, R. E. Cowley, M. F. Qayyum, R. A. Himes, M. A. Siegler, C. D. Moore, B. Hedman, K. O. Hodgson, S. Fukuzumi, E. I. Solomon and K. D. Karlin, *J. Am. Chem. Soc.*, 2013, **135**, 16454-16467.

58. J. S. Woertink, L. Tian, D. Maiti, H. R. Lucas, R. A. Himes, K. D. Karlin, F. Neese, C. Wurtele, M. C. Holthausen, E. Bill, J. Sundermeyer, S. Schindler and E. I. Solomon, *Inorg. Chem.*, 2010, **49**, 9450-9459.

59. R. L. Peterson, R. A. Himes, H. Kotani, T. Suenobu, L. Tian, M. A. Siegler, E. I. Solomon, S. Fukuzumi and K. D. Karlin, *J. Am. Chem. Soc.*, 2011, **133**, 1702-1705.

60. J. W. Ginsbach, R. L. Peterson, R. E. Cowley, K. D. Karlin and E. I. Solomon, *Inorg. Chem.*, 2013, **52**, 12872-12874.

61. T. Tano, Y. Okubo, A. Kunishita, M. Kubo, H. Sugimoto, N. Fujieda, T. Ogura and S. Itoh, *Inorg. Chem.*, 2013, **52**, 10431-10437.

62. A. Kunishita, M. Z. Ertem, Y. Okubo, T. Tano, H. Sugimoto, K. Ohkubo, N. Fujieda, S. Fukuzumi, C. J. Cramer and S. Itoh, *Inorg. Chem.*, 2012, **51**, 9465-9480.

63. A. Kunishita, M. Kubo, H. Sugimoto, T. Ogura, K. Sato, T. Takui and S. Itoh, *J. Am. Chem. Soc.*, 2009, **131**, 2788-2789.

64. S. Kim, J. Y. Lee, R. E. Cowley, J. W. Ginsbach, M. A. Siegler, E. I. Solomon and K. D. Karlin, *J. Am. Chem. Soc.*, 2015, **137**, 2796-2799.

65. B. N. Sanchez-Eguia, M. Flores-Alamo, M. Orio and I. Castillo, *Chem Commun (Camb)*, 2015, **51**, 11134-11137.

66. K. B. Alwan, E. F. Welch, R. J. Arias, B. F. Gambill and N. J. Blackburn, *Biochemistry*, 2019, **58**, 3097-3108.

67. A. T. Bauman, E. T. Yukl, K. Alkevich, A. L. McCormack and N. J. Blackburn, *J. Biol. Chem.*, 2006, **281**, 4190-4198.

68. M. J. Baldwin, D. E. Root, J. E. Pate, K. Fujisawa, N. Kitajima and E. I. Solomon, *J. Am. Chem. Soc.*, 1992, **114**, 10421-10431.

69. N. Kitajima, in *Bioinorganic Chemistry of Copper*, eds. K. D. Karlin and Z. Tyeklar, Chapman & Hall, New York, 1993, pp. 251-263.

70. K. A. Magnus, B. Hazes, H. Ton-That, C. Bonaventura, J. Bonaventura and W. G. J. Hol, *Proteins Struct. Funct. Genet.*, 1994, **19**, 302-309.

71. K. Rudzka, D. M. Moreno, B. Eipper, R. Mains, D. A. Estrin and L. M. Amzel, *J. Biol. Inorg. Chem.*, 2013, **18**, 223-232.

72. C. D. Kline, M. Mayfield and N. J. Blackburn, *Biochemistry*, 2013, **52**, 2586-2596.

73. C. D. Kline and N. J. Blackburn, *Biochemistry*, 2016, **55**, 6652-6661.

74. O. Einarsdottir, P. M. Killough, J. A. Fee and W. H. Woodruff, *J. Biol. Chem*, 1989, **264**, 2405-2408.

75. A. T. Bauman, M. Ralle and N. Blackburn, *Protein Expression and Purification*, 2007, **51**, 34-38.

76. E. F. Welch, K. W. Rush, R. J. Arias and N. J. Blackburn, *Biochemistry*, 2022, **61**, 665-677.

Data Availability. The data supporting this article are included as Figures and Tables either in the main article or as Supplementary Information. Raw EXAFS, EPR and UV/vis spectral data are archived on cloud-based data storage systems and are available from the corresponding author on request.